



Coupled models for polymer synthesis and rheology to determine branching architectures and predict flow properties

Chinmay Das¹ · Wenjun Li² · Daniel J. Read¹ · Johannes M. Soulages²

Received: 26 October 2018 / Revised: 19 February 2019 / Accepted: 19 February 2019 / Published online: 8 March 2019
© The Author(s) 2019

Abstract

Advance in computational rheology allows for *in silico* predictions of the viscoelastic responses of arbitrarily branched polymer melts. While detailed branching structure is required for the rheology predictions, rheology itself is often the most sensitive tool to detect low levels of branching. With rheological experiments and computational modeling of a set of nominally linear and model comb ethylene-butene copolymers, we show that coupled models for the synthesis and rheology can integrate diverse measurements, incorporating inherent experimental uncertainties. This approach allows us to achieve tight bounds on the branching structures of the constituent molecules. Next, we numerically explore the effects of the numbers and molar masses of side arms in comb polymers on the viscoelastic responses in both the linear and nonlinear regimes. Such computational exploration can aid in designing specific polymers suitable for a given processing scenario.

Keywords Polymer rheology · Long-chain branching · Cross-linked polymer · Structure-rheology relations

Introduction

The presence of long-chain branches (LCB) has profound effects on the rheological properties of polymer melts (Hatzikiriakos 2000), often aiding processing by impacting favorable properties such as higher shear thinning and increased extension hardening (Gortis et al. 2004; Münstedt et al. 2005; Sebastian and Dearborn 1983). The flow properties are affected in a complex fashion by the detailed branching topology of the molecules present in the melt. Even the linear flow response of branched polymers exhibits nontrivial dependence on the details of the branching architectures. This complexity is influenced by the hierarchical nature of the stress relaxation (McLeish 1988) within individual molecules, as well as by the coupling of relaxation of different molecules from the softening of the entanglement constraints (Marrucci 1985; Ball and McLeish 1989)

(dynamic dilution) from the fast relaxing segments. For idealized branching architectures, analytical expressions for the stress decay within the tube theory (Doi and Edwards 1986; de Gennes 1971) are feasible. However, even the most careful synthesis of model branched architectures results in both the molar mass polydispersity and architectural polydispersity from the placement and the number of branches in a given molecule (Hutchings et al. 2012; Li et al. 2011; Snijkers et al. 2011). Computational schemes (Larson 2001; Das et al. 2006; van Ruymbeke et al. 2006; Read et al. 2011; Das et al. 2014) have been developed, which consider a representative set of differently branched molecules and numerically solve the coupled relaxation of the molecules after a small step strain. These models have been successful in predicting the viscoelastic responses of a number of model and industrial polymers in the linear and nonlinear flow.

Often, the agreement between the rheological measurements and the numerical predictions for branched polymers is limited by the knowledge of the branching topology of the molecules in a particular sample. In favorable cases, recent developments in specialized separation techniques (Chang 2005) allow for direct experimental determination of the various branched species in a particular sample (Hutchings et al. 2012; Li et al. 2011; Snijkers et al. 2011). However, such separation techniques remain difficult, are not applicable to all

✉ Chinmay Das
C.Das@leeds.ac.uk

✉ Daniel J. Read
D.J.Read@leeds.ac.uk

¹ School of Mathematics, University of Leeds, Leeds LS2 9JT, UK

² ExxonMobil Research and Engineering, Annandale, NJ 08801, USA

chemistries, and require temperature variations individually tuned for each sample.

Since a small number of long-chain branches can have significant effect on the flow properties, the inverse problem of determining the branching structure from rheology seems natural. Determination of the molar mass distributions of linear polymers from their rheological responses has been relatively well-developed (Carrot and Guillet 1997; Liu et al. 1998; Le'onardi et al. 2002; Pattamaprom et al. 2008), especially for polymers with broad and smooth molar mass distributions where double reptation theory (des Cloizeaux 1988) provides a good description. However, determining the structure from rheology alone remains a hard—and likely impossible—problem for branched polymers. Over a limited frequency range, a very large number of possible structures can have the same viscoelastic response. Therefore, rheology can only be used to determine the structure if one limits the possible structures within a restricted class of branching from the knowledge of the synthesis process (Takeh et al. 2011; van Ruymbeke et al. 2014; Dealy et al. 2018).

Since most reactions for synthesizing branched polymers generate a statistical distribution of differently branched molecules, a numerical scheme that integrates some aspects of the synthesis process in the complex mixture of molecules becomes essential to faithfully describe and predict the topological structures and the flow properties of branched polymers. As we show in this work, experimental uncertainties imply that, in general, more confidence is gained regarding the branching structures of the constituent molecules by modeling both the synthesis and the flow properties together in a single, coupled, scheme.

Hence, coupled models for synthesis and polymer relaxation for branched polymers can be applied in to achieve (at least) two distinct, but complementary goals. The first is in a direct, predictive mode: given a set of polymers synthesized under certain specific conditions, the coupled models can be used to predict the resulting polymer architectures and flow properties. But a second possibility is to use the models to assimilate a diverse set of information, including both experimental measurements (incorporating experimental uncertainties) and knowledge about the synthesis method (which also contains uncertainties in terms of rate a parameters and imperfections such as side reactions). Given the available information, the models can be used to infer the most likely branching architectures present in a particular sample.

In this paper, we illustrate both the above applications, focusing on two classes of polymer architecture: (i) branched polymers synthesized by single-site metallocene catalysts, and (ii) comb polymers. This work is organized as follows: In the following section, we illustrate how diverse experimental data can be assimilated to obtain information on branching structure, through two examples. We show experimental characterizations using size-exclusion chromatography (SEC) and

small amplitude oscillatory shear (SAOS) for three ethylene-1-butene copolymers synthesized in a CSTR (continuous stirred tank reactor) with metallocene catalysts (Braunschweig and Breitling 2006; Britovsek et al. 1999). Except for the low frequency elastic modulus, all measured properties of these polymers suggest the absence of any long-chain branching. However, the combined modeling of the synthesis and rheology shows that the low-frequency moduli for these polymers can only be described with a small but nonzero fraction of long-chain branches, at a level below the detection limits of SEC and NMR (nuclear magnetic resonance) spectroscopy. Next, we consider four hydrogenated polybutadiene comb polymers synthesized by Hadjichristidis et al. (2000) and rheological responses measured by Lohse et al. (2002). Chemically, these polymers are identical to ethylene-1-butene copolymers. We show that the coupled models for structural synthesis and rheology provide tight bounds in the determination of the average number of side arms in these polymers, and also that the different measurements can only be reconciled by assuming significant cross-linking in two of these samples.

In the next section titled “[Effect of comb arms on the flow properties](#)”, we apply the rheology model in a direct predictive mode, to explore the range of possible flow properties of idealized (but still realistic) comb polymers without cross-linking. Approximate analytical models are available (Daniels et al. 2001; Inkson et al. 2006; Kapnistos et al. 2005) that can predict the linear viscoelastic response for comb polymers with a *fixed* number of arms. However, the most common synthesis of comb polymers results in a statistical distribution of molecules with Poisson distributed side arms (Chambon et al. 2008). Proper accounting of this variability in terms of the number and positioning of side arms in these polymers requires numerical investigation. Besides the shear response in the linear regime, we also calculate the non-linear responses for these idealized combs in an extensional flow. Using a number of scalar measures to characterize the shear and extensional behaviors of the comb polymers at a fixed shear/extension rate, we show that a small number of comparatively short side arms have the strongest effect on the shear viscosity enhancement, the comb architecture does not show strict extensional hardening (increasing extensional viscosity with increased extension rate), and that at a fixed average side arm number, there is an optimum molar mass of side arm to achieve the maximum extensional hardening. Finally, we end this paper with a summary of the findings and a discussion.

For the modeling of polymer synthesis and rheology in this work, we used a slightly modified version of branch-on-branch rheology software (Das et al. 2006, 2014; Das and Read 2018). The details of this computational rheology algorithm have been extensively described elsewhere (Das et al. 2006, 2014). The assumptions and parameters for relaxation

in the computation follow the previously used values in the literature. In particular, we consider that the tube dilation exponent α to be 1, and the parameter p^2 , characterizing the hop size of a branch point with localized friction from relaxed side arm (Frischknecht et al. 2002), to be 1/40 (Das et al. 2006). The numerical ensembles of polymer molecules were generated mimicking the polymer synthesis processes via Monte Carlo algorithms using in-built codes within the bob-rheology software. For example, the software contains options for generating comb molecules with randomly placed arms and ensembles of branched molecules synthesized via metallocene polymerization (Das et al. 2006). Unless stated differently, we generate 50,000 molecules to capture faithfully the small weight fractions of highly branched and low-probability molecules from our stochastic sampling. However, this number of molecules will typically result in long computations for the rheology prediction. To accelerate the computation speed, a representative set of 5000 molecules is sampled from the original 50,000, chosen uniformly across the spectrum of molar mass. To account for the discarded molecules, each chosen molecule is given an appropriate weight in the rheology calculation to compensate for molecules of similar weight discarded during the sampling procedure.

Assimilating multiple experimental measurements to determine branching architectures

Different experimental techniques can be used on a given polymer sample to find certain average properties of the constituent molecules. Size-exclusion chromatography (SEC), light scattering (LS), or membrane osmometry can all be used to measure the molar mass distribution or some moments of the molar mass distribution. The number of long-chain branches can be estimated via NMR spectroscopy (Randall 2006). With the knowledge of the molar mass of the molecules and the segments, the NMR measurements provide the average number of branches per molecule. The radius of gyration and intrinsic viscosity can be compared to known values for linear molecules having the same molar mass, and any reduction in the ratios from unity can be used as a signature for branching (Wang et al. 2004) and can be related to LCB content subject to assumptions about the branching architectures (Zimm and Stockmayer 1949). However, the sensitivity of all these solution-based measurements is limited to LCB contents greater than 1 LCB per 10^4 carbons (Randall 2006; Janzen and Colby 1999). Melt viscosity is more sensitive to the molecular weight, and deviations from known behavior of linear polymers of the same molar mass have been proposed (Janzen and Colby 1999; Shroff and Mavridis 1999) to qualitatively indicate the presence of much smaller numbers of LCB than

measurable via solution-based methods. The sensitivity in measuring the LCB content from viscosity depends on the typical number of entanglements per molecule and therefore on the ratio of molar mass to entanglement molar mass. Here, we implicitly assume that the polymers we are dealing with are typical commercial polyethylene with the average number of entanglement per molecule being order 100, and the typical branches having similar molar masses as the linear molecules. For polymers with fewer entanglements, the sensitivity in LCB estimates from viscosity can be far lower (van Ruymbeke et al. 2006a). To circumvent the difficulty in measuring zero-shear viscosity, the presence of LCB may be detected by comparing the measured oscillatory shear response at finite frequency with the predicted oscillatory shear response of linear polymers having the same measured molar mass distribution; deviations between the measured and predicted response have been used to indicate the presence of LCB (van Ruymbeke et al. 2005). Such melt viscosity-based indicators rely on the deviation from linear polymer rheology. But without a priori knowledge about the branching architectures and a method to predict the rheology of such branched polymers, they cannot quantify the abundance of LCB. Also, a priori it is difficult to judge if different measurements on a sample are consistent within the experimental uncertainties. However, a numerical scheme could potentially offer a robust method to determine the underlying molecular architectures by assimilating all the available experimental measurements. In this section, we use a set of metallocene catalyzed polymers with very low levels of branching and a set of model comb polymers with varying levels of branching to determine the molecular architectures by matching the predictions from numerical models to the experimental measurements.

Sparsely branched metallocene polymers

In this work, we consider three ethylene-butene polymers synthesized with a metallocene catalyst and with different weight fractions of butene as comonomer. The details of the experiments used to obtain the experimental data in this section are presented in the “Appendix” section. The butene contents, determined from NMR, and the molar mass moments, determined from size-exclusion chromatography and multi-angle laser light scattering (SEC-MALLS), are shown in Table 1 (left). The full molar mass distribution is shown in the left-hand panels of Fig. 1. The lines in these plots show the predictions from ideal Flory distributions matching the experimentally determined M_w . Polymerization with metallocene catalysts in CSTR is relatively well studied (Braunschweig and Breitling 2006; Britovsek et al. 1999; Soares and Hamielec 1996; Read and McLeish 2001) and, in the absence of branching, produces Flory-distributed polymers with the

Table 1 Characterization of metallocene ethylene-1-butene copolymers. Molar masses are in kg/mol

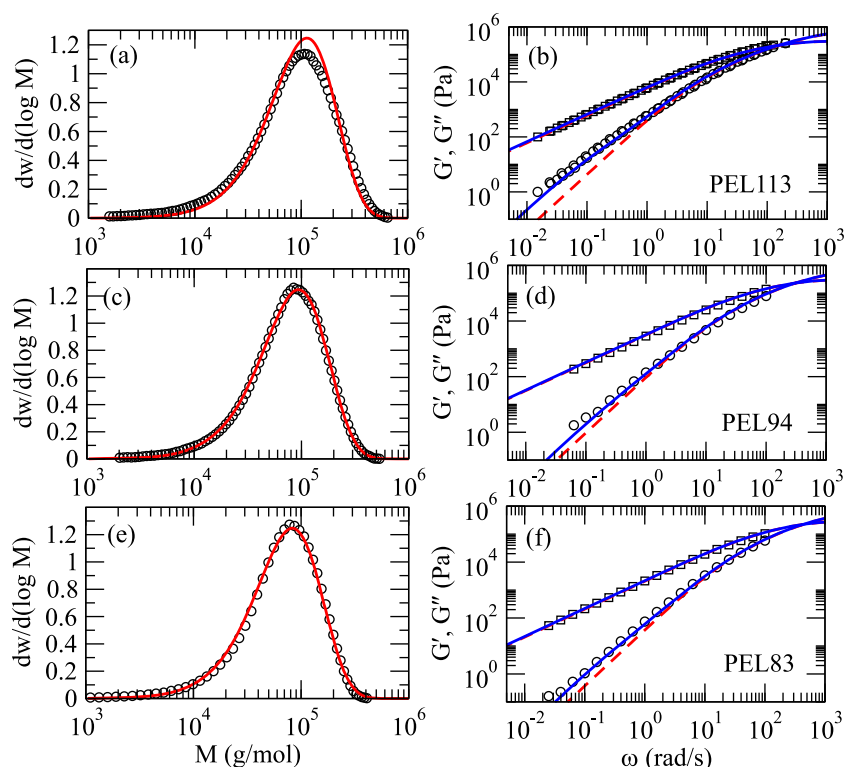
Sample	NMR	SEC-MALLS					Model parameters			
	Wt% C4	M_N	M_W	M_Z	PDI	M_Z/M_W	m_b	Wt% star	LCB/ 10^3 mol	LCB/ 10^6 C
PEL113	7.6	45.8	113	181	2.47	1.6	14.55	1	3.3	0.8
PEL94	9.9	46.5	94	141	2.02	1.5	14.73	0.5	1.7	0.5
PEL83	12.6	35.4	83	122	2.35	1.5	14.94	0.7	2.3	0.8

polydispersity index (PDI) of 2.0. The polydispersity index for PEL94 is close to this ideal value. The other two samples show broader distribution with PDI = 2.35 for PEL83 and PDI = 2.47 for PEL113, respectively. The ratio M_Z/M_W is close to 1.5 for all the samples, showing that the deviation of the molar mass distribution from the idealized Flory distribution is because of slightly higher abundance of lower molar mass species. The same conclusion can be obtained by noting that the predictions from Flory distributions in Fig. 1 consistently fall below the experimental data at low molar mass end. The SEC-LS profiles and the scaling of the zero-shear viscosity of these samples are consistent with the expectations for linear polymers with similar comonomer content. It is worth noting that no signatures of LCB were detected within the noise level from NMR spectroscopy using a cryoprobe for these three polymer samples.

For the moment assuming that the polymers have no long-chain branches, predicting the flow properties from the

computational model requires a numerical ensemble of molecules consistent with the measured molar mass distribution. From the SEC separation, we determined the concentration (from differential refractive index detector) and the weight-averaged molar mass (from light scattering) of each elution volume separately to determine the weight fractions of the different molar mass molecules in the samples. This discrete distribution of linear molecules of different molar masses was directly used to compute rheology predictions using the BoB software. Two chemistry dependent parameters, the entanglement molar mass M_e and the entanglement time τ_e are required for the calculations. For ethylene- α -olefin copolymers, phenomenological rules connect these parameters to the effective backbone molar mass defined as the effective molar mass per backbone carbon incorporating the side group monomer masses (Fetters et al. 2002; Chen et al. 2010; Stadler and Münstedt 2008). The backbone molar masses (m_b) computed from the comonomer contents are shown in Table 1. The

Fig. 1 Molar mass distributions (a, c, e) and small amplitude oscillatory shear responses (b, d, f) of PEL113 (a, b), PEL94 (c, d), and PEL83 (e, f)



entanglement molar mass for each sample was calculated from the backbone molar mass as $M_e = 1.12 \times \left(\frac{M_b}{14}\right)^{3.49}$ kg/mol (Fetters et al. 2002). Here, we assumed that the M_e for ethylene homopolymer is 1.12 kg/mol (Das et al. 2006). The entanglement time at the experimental temperature of 190 °C was calculated as $\tau_e = 4.4 \times 10^{-9} \times \left(\frac{M_b}{14}\right)^{16.054}$ s (Chen et al. 2010). The value of τ_e is consistent with the previous modeling for ethylene homopolymers (Das et al. 2006), once the shift factor for the different temperatures used in the earlier study is accounted for. For calculating the plateau modulus, a density of 0.76 g/cc was used for all these three samples.

The right-hand panels in Fig. 1 show the viscoelastic moduli from the small amplitude oscillatory shear experiments (symbols) and the predicted values based on linear polymers with the measured molar mass distribution (dashed lines). The predictions capture the crossover frequency and the viscous frequency response well. However, at the low frequencies, the experimental elastic moduli show significantly larger values compared to the predictions. Metallocene catalysts are capable of forming long-chain branched molecules by incorporating macromonomers generated from β -hydride elimination (Soares and Hamielec 1996). The fractions of such long-chain branched molecules in our samples are necessarily small because only the low-frequency elastic modulus shows significant deviation from the predictions that assume absence of long-chain branches. At low levels of branching, we only need to consider molecules with a single branch point. For synthesis with a metallocene catalyst in a CSTR, the molecules with a single branch point are star-branched molecules with each of the arms separately having the same M_w as the linear polymers and following independent Flory distributions (Soares and Hamielec 1996; Read and McLeish 2001). The solid lines in the right-hand panels of Fig. 1 are linear rheology predictions based on an ensemble of polymer molecules that include (i) linear molecules determined from the molar mass distribution and (ii) a small fraction consisting of star polymers in which each star arm is Flory distributed with average molar mass fixed by the linear polymer M_w . The weight fractions of the star polymers required to match the elastic modulus are shown in Table 1 (right). Note that the addition of these small quantity of star polymers (≤ 1 wt%) does not change the predictions of viscous modulus appreciably. From the weight fraction of the star polymers, we can estimate that the samples have less than one long-chain branch per million carbons—a level far below the detection sensitivity of NMR.

In principle, it would also be possible to match the linear rheology data by introducing a small fraction of extremely high molecular weight linear polymers. However, the observed feature in the storage modulus indicates material that is relaxing on times of order 10^4 longer than the characteristic relaxation time of the material; fitting with linear molecules alone would require introducing molecules at least 10 times

longer than suggested from SEC data, for which there is no real justification: the Flory distribution matches the SEC data well. In contrast, as noted above, the synthesis mechanism provides a natural explanation for a small fraction of star polymers of similar molecular weight to the majority linear molecules; hence, we consider the small fraction of stars to be by far the most likely explanation for the observed rheology.

The predictions based on the linear polymers alone and with the star-branched fraction differ in zero-shear viscosity by less than 10%. Thus, the viscosity difference itself is experimentally measurable with confidence. However, to use the zero-shear viscosity itself as an indicator would require less than 3% uncertainty in the measured molar mass. While this is possible in principle, experimental evidence (D’Agnillo et al. 2002; Sloommaekers et al. 1991) suggests much larger uncertainties of the measured molar mass. We consider that the present approach is far more robust with respect to uncertainties in the molar mass distribution. Our approach is similar to reference (van Ruymbeke et al. 2005) in that we try to look for deviation of the oscillatory shear responses from the predictions based on the assumption of linear polymers alone. The novel point of our work is to incorporate the next possible branched candidate molecules from the knowledge of synthesis and to quantify the LCB content. While we have used only star-branched polymers in our analysis in Fig. 1, the LCB content can be used in a Monte Carlo simulation for generating branched metallocene polyethylene. In order to check this, we created an ensemble of branched polyethylene with the experimentally determined weight average molecular weight M_w and LCB content from our fit of the elastic modulus, using a previously published algorithm (Das et al. 2006) for branched polymers created through single-site metallocene catalysis. This ensemble does not exactly match the measured GPC data at the low molar mass end, where experimental data shows a greater fraction of low molar mass molecules than would be expected from a Flory distribution. However, this small fraction of excess low molar mass linear molecules does not affect the rheology significantly at low frequencies. The rheology predictions using this ensemble of molecules are virtually identical to the numerical ensemble containing only linear and star-branched molecules. This is not surprising since the weight fraction of twice branched molecules (H-polymers) is approximately two orders less than that of star-branched molecules at these low levels of branching.

Model hydrogenated polybutadiene combs

We next turn our attention to a set of model comb polymers. Details of the synthesis of these combs have been reported by Hadjichristidis et al. (2000) and rheological measurements reported by Lohse et al. (2002). For these comb polymers, anionic polymerization was used to synthesize the

polybutadiene backbone, attachment points were created on the backbone with dimethylchlorosilane, and separately synthesized living segments were added in excess to form the side arms. Finally, these samples were purified to remove the unreacted excess arms. Molar mass at each step of the synthesis was monitored, and the average numbers of the branch points were estimated from both the molar masses of the components and the entire combs as well as from NMR. The polybutadiene combs were hydrogenated to give ethylene-1-butene chemistry. All the combs had between 9 and 10 wt% butene. SEC-LS measurements were used to calculate the molar masses and the radius of gyration contraction factor (g -factor) for the hydrogenated combs, which are reproduced from Hadjichristidis et al. (2000) in Table 2.

As can be seen from Table 2, the estimates for the number of arms from NMR and SEC are not identical. Using SEC/osmometry measurements of the polybutadiene segments and the polybutadiene combs, the numbers of arms were determined as $n^a = (M_N^c - M_N^b) / M_N^a$. Routine measurements for molar mass carry significant variability (D'Agnillo et al. 2002; Sloodmaekers et al. 1991). The separation based on the hydrodynamic size of branched polymers and the necessity of choosing the integration window somewhat arbitrarily (Sun et al. 2004) introduce yet more uncertainty. Assuming a 5% uncertainty in determining the molar masses, the error estimates in determining the number of arms for these combs are shown in Table 3 (left). For PEC(100)–(5)₂, we expect a 100% uncertainty in determining the number of arms, making the estimate from SEC of two side arms consistent with lack of branching from NMR for this particular comb. Note that our choice of the uncertainty in the molar mass is arbitrary, and a larger uncertainty is often reported in the literature (D'Agnillo et al. 2002; Sloodmaekers et al. 1991); hence, the actual uncertainty in arm number could be larger. Also shown in Table 2 are the estimated backbone and side arm molar masses for the hydrogenated combs assuming full hydrogenation.

We reproduce the oscillatory shear results from reference (Lohse et al. 2002) in Fig. 2, along with fits from our

computational modeling. The experimental data shows some thermorheological complexity and does not cover high enough frequencies to reach the plateau region, so there is some uncertainty in the data, especially at higher frequencies. All data shown is time-temperature shifted to the same reference temperature of 190 °C. For the PEC(87)–(5)₃ and PEC(100)–(5)₁₂ samples, most of the interesting features of the data are covered by the experimental frequency range of 0.01 and 100 rad/s at the reference temperature, and our conclusions drawn for these samples would remain intact if we included only the data taken at 190 °C. PEC(100)–(5)₂ and PEC(97)–(23)₂₆ require data beyond those taken at 190 °C to capture the regions of interest. However, though different activation energies were required to superpose different temperature data for these two samples, both samples show good superposition of the different temperature measurements. Hence, the choice of any other reference temperature would not have changed our conclusions, except for requiring different τ_e for the different samples to account for the different activation energies. As it is, choosing the same reference temperature encourages us to use the same τ_e for all samples in our modeling rather than treating it as a separate fitting parameter for each sample. For our modeling, we assume 9.5% butene content and use $M_e = 1327$ g/mol and $\tau_e = 9.62 \times 10^{-9}$ s. Since the plateau region is not attained in the data, it is difficult to assess whether the model is predicting the plateau perfectly, though there may be a slight overprediction evident in Fig. 2 a and b.

The data for PEC(100)–(5)₂ (Fig. 2a) is qualitatively similar to the metallocene polymers in the previous subsection. The clear reptation peak requires a backbone molar mass of 95 kg/mol instead of 104 kg/mol suggested from SEC. Such a difference is justified within the uncertainty in molar mass determination. Note that the backbones for the different combs came from different batches of synthesis and similar variations were present in the repeat GPC measurements. A smaller value for the backbone for the PEC(100)–(5)₂ is quoted by Lohse et al. (2002). The behavior of the elastic modulus at

Table 2 Molar mass and estimated numbers of arms of polybutadiene precursors and hydrogenated combs. Molar masses are in kg/mol. (Adapted with permission from *Macromolecules*, 2000, 33, 2424–2436. Copyright (2000) American Chemical Society)

Sample	Polybutadiene precursors							Fully hydrogenated polybutadiene combs			
	arm		backbone		comb			n^a	M_N	M_W	g
	M_N^a	M_W^a	M_N^b	M_W^b	M_N^c	M_W^c					
					SEC	NMR					
PEC(100)–(5) ₂	5.2	5.3	96.8	99.7	109	111	2	0	105	105	1.00
PEC(97)–(23) ₂₆	NM	23.5	NM	97	NM	612	22	26	660	735	0.32
PEC(87)–(5) ₃	4.5	NM	87	90	106	107	4	3	NM	NM	NM
PEC(100)–(5) ₁₂	5.2	5.3	96.8	99.7	173	178	15	12	166	171	0.70

Table 3 Estimated parameters for the polyethylene combs

Sample	Hydrogenated combs*			Model parameters			g^{id}	% cross-linked
	M_{W}^{a}	M_{W}^{b}	n^{a}	M_{W}^{a}	M_{W}^{b}	n^{a}		
PEC(100)–(5) ₂	5.5	104	2 ± 2	5.5	95	0.1 (0.07–0.14)	0.996	
PEC(97)–(23) ₂₆	24.4	101	22 ± 1.8	24.4	101	20 (19–22)	0.25–0.28	
PEC(87)–(5) ₃	4.8	93	4 ± 2.2	4.8	95	2.9 (2.5–3.4)	0.87–0.88	5 (3–7)
PEC(100)–(5) ₁₂	5.5	104	15 ± 2.7	5.8	104	7.5 (7–8)	0.68–0.70	20 (15–25)

*Molar masses estimated from polybutadiene precursors by assuming complete hydrogenation, error estimates in the measured number of arms from SEC data assumes ± 5% uncertainty in the measurements of the molar masses of precursors and comb polymers

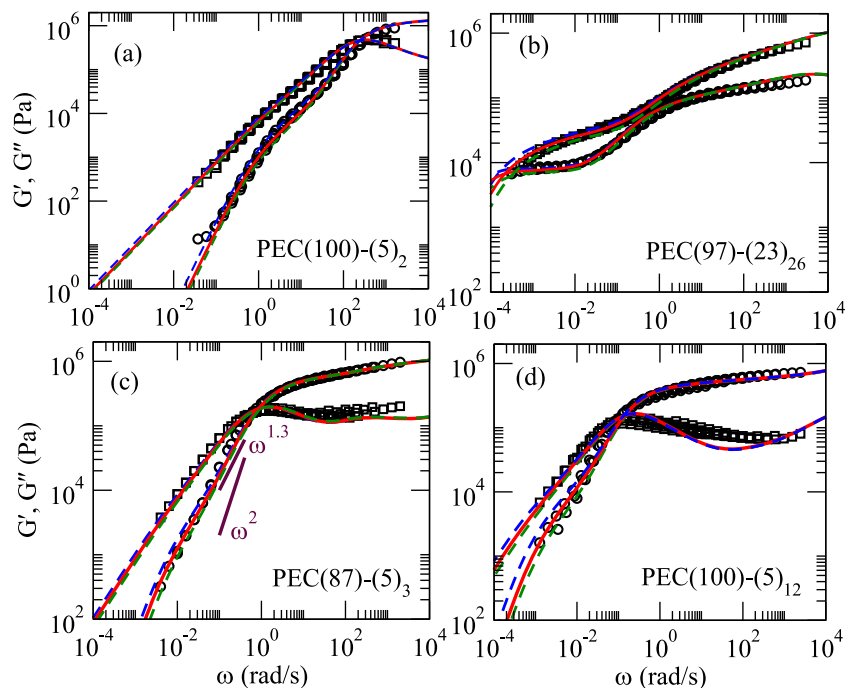
frequencies lower than the frequency for the reptation peak is consistent with $n^{\text{a}} = 0.1$ (solid line), with the likely bound $0.07 \leq n^{\text{a}} \leq 0.14$ (dashed lines).

The longer (24.4 kg/mol) side arms in PEC(97)–(23)₂₆ show separate features associated with the side arm relaxation (around 1 rad/s) and eventual reptation (around 3×10^{-4} rad/s) within the experimental measurement window (Fig. 2b). The large weight carried by the side arms results in reduced modulus at the reptation frequency that depends on the number of side arms. The experimental data is consistent with $19 \leq n^{\text{a}} \leq 22$, slightly less than the NMR estimate of 26 arms but consistent with the SEC estimate of 22 ± 1.8 . We can use the numerical ensemble of molecules to calculate the ideal radius of gyration contraction factor. The calculated g -value of 0.25–0.28 is slightly smaller than the measured value of 0.32. With the model correctly predicting the timescale for arm retraction (behavior close to 1 rad/s), the number of arms decide two different low-frequency features (the timescale of reptation

and the modulus at reptation). Since $n^{\text{a}} \approx 20$ describes both these features simultaneously, the fitting also can be viewed as a validation on our choice of the value of the hopping parameter p^2 .

Figure 2 c shows the viscoelastic response of PEC(87)–(5)₃. We have drawn two power-law lines to show that the storage modulus beyond the reptation peak shows a power of 1.3 instead of the terminal power of 2. Such behavior deviating from power law 2 expected for terminal relaxation suggests highly branched structures besides the assumed comb architecture. It had been noted earlier (Ferryhough et al. 2001) that during synthesis, some of the backbones can be cross-linked during the hydrosilation step in the presence of trace water. In our numerical scheme, we allow for such cross-linking by randomly joining two numerical combs along the backbone and fit the experimental viscoelastic response by varying the number of arms and the fraction of cross-linked molecules. The experimental data is consistent with comb

Fig. 2 Experimental viscoelastic responses (symbols) from Lohse et al. (2002) shifted to reference temperature 190 °C and computational predictions (lines) for the polyethylene combs



molecules with 2.5–3.4 side arms and 3–7 wt% cross-linked material. Again, the number of arms is consistent with the SEC measurement within the error estimates.

The elastic response for PEC(100)–(5)₁₂ shows similar nonterminal slope as with PEC(87)–(5)₃ (Fig. 2d). The experimental data for this sample show lack of time-temperature superposition (TTS) more prominently than the other three samples. Our modeling suggests significant (15–25 wt%) cross-linked material and number of arms between 7 and 8. Our predicted number of arms for this sample is much lower than that calculated based on SEC data ($n^a = 15 \pm 2.8$), or from NMR ($n^a = 12$). However, the calculated g -factor (0.68–0.7) agrees with the measured radius of gyration contraction factor of 0.7. This suggests that the estimates based on SEC or NMR were higher because of the assumed perfect comb structure: a significant fraction of linked combs would increase the measured average molar mass of the samples and so increase the calculated number of arms per molecule if a perfect comb is assumed. The poor time-temperature superposability for this sample offers a further, independent, qualitative indication of cross-linked molecules containing branch-on-branch architectures in this sample (Wood-Adams and Costeux 2001).

Effect of comb side arms on the flow properties

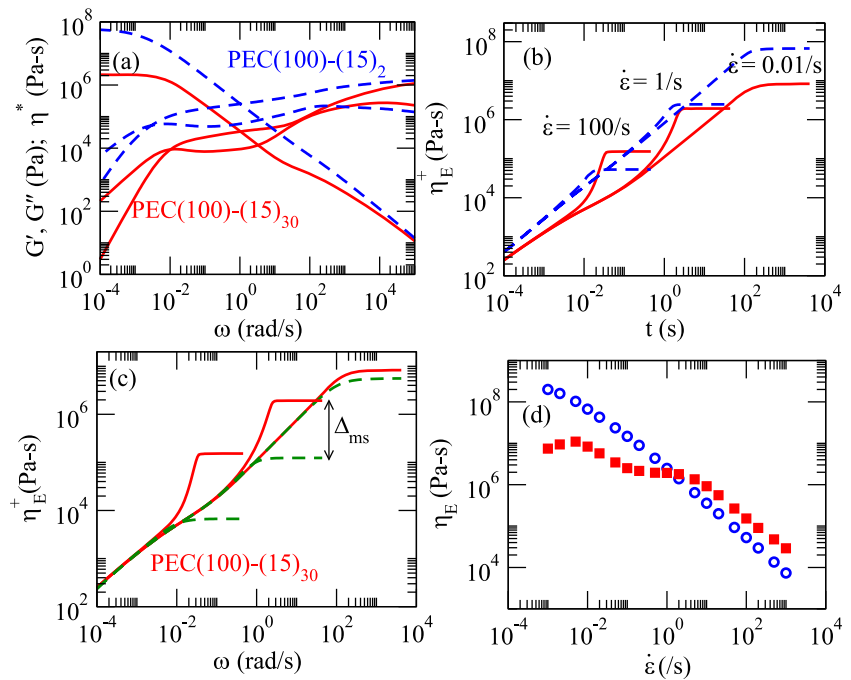
As we showed in the previous section, provided experimental uncertainties are taken into account, and coupled numerical models can be used to find the most likely structures present in a particular melt taking account of different analytical and rheological measurements. The coupled models can also be used to computationally explore the effect of structures on rheology. In this section, we consider idealized comb structures (that is, excluding the possibility of cross-linked molecules, but including the variability in the position and number of the side arms present from polymer synthesis) and study the effect of the number and molar masses of the side arms on the flow properties. We keep the backbone molar mass as 100 kg/mol (~75 entanglements) and use the parameters for polyethylene with 9.5 wt% butene as used and discussed above. The number of arms per molecule was varied between 0.02 (1 LCB per 50 molecules) and 30. The molar mass of the side arms was varied between 5 (~3.8 entanglements) and 50 kg/mol (~38 entanglements). Even at the highest density of side arms, the branch points are separated by about 2.5 entanglements, and all the backbones remain entangled in the dilated tube once the side arms have relaxed. This ensures that the assumptions on which the computational scheme is built remain valid. Besides the linear response, we also calculate the nonlinear extensional responses in this part of the work. For

nonlinear rheology predictions, the calculation utilizes a set of pom-pom modes (McLeish and Larson 1998) with the orientation and stretch relaxation times and the effective maximum stretch at a given flow rate (priority variables) determined by following the relaxation history after a small step strain. Details of the algorithm for this assignment of pom-pom modes are available in reference (Das et al. 2014).

In Fig. 3 a, we show predictions of the linear viscoelastic responses for two comb polymers with the average number of arms being either 2 or 30, but with the same molar mass of the side arms (15 kg/mol). The large number of side arms allows for significantly more dynamic dilution for the 30-arm comb as compared to the 2-arm comb, and the zero-shear viscosity for the 30-arm comb is approximately 1/30 of that of the 2-arm comb. Figure 3 b shows predictions of the stress growth coefficients in uniaxial extension (transient extensional viscosities) at extension rates 0.01, 1, and 100/s. At low rates, the steady-state extensional viscosity for the 30-arm comb is lower than that of 2-arm comb by a factor close to the ratio of their respective zero-shear viscosities. However, at higher rates, the 30-arm comb shows higher extensional viscosity than the 2-arm comb. In Fig. 3 c, we compare the extensional viscosity of the 30-arm comb with a model that retains the same pom-pom modes as the original ensemble but does not permit stretch of the pom-pom modes, i.e., the stretch variable in the pom-pom equations is set equal to one throughout the computation (see below for a justification for such a comparison). With increasing extensional rate, the predicted extensional viscosity shows much higher values compared to the predictions without chain stretch. Fig. 3 d shows the steady extensional viscosity of the two combs as a function of the extensional rates. Over a range of rates (< 10/s), the 30-arm comb shows less extension thinning than the 2-arm comb.

While the complex flow responses represented in Fig. 3 for the two different combs give detailed information on the flow responses under different shear/extension conditions, such detailed information makes it difficult to compare among large numbers of different polymer architectures. Instead, we define a set of scalar measures that depend on the shear/extension rate and use these quantities to visually compare the response of different samples by restricting our attention to a single shear/extension rate. In the results below, we assume this relevant shear/extension rate to be 1/s. If in a particular application, the flow rates involved are very different from this rate, one would need to calculate (or measure) the indicators at the corresponding relevant rate. In addition to the commonly used complex viscosity and steady state extensional viscosity evaluated at the relevant rate, we use a set of further scalar measures which we have found to be useful and which we describe in the following paragraphs.

Fig. 3 **a** Viscoelastic modulus and complex viscosities, **b** start-up stress growth coefficients in uniaxial extension (transient extensional viscosities) for hypothetical comb polymers with 100 kg/mol backbone, 15 kg/mol side arms, and with the average number of arms being either 30 (solid lines) or 2 (dashed lines). **c** Excess extensional viscosity due to molecular stretching in PEC(100)–(15)₃₀, and **d** steady-state extensional viscosity as a function of extension rate for PEC(100)–(15)₃₀ (filled squares) and PEC(100)–(15)₂ (open circles)



Over a limited shear rate, $\dot{\gamma}$, the shear viscosity can be expressed as a power-law

$$\eta = m \dot{\gamma}^{n-1}$$

defining the shear-thinning index n and the consistency m . Experimentally, polymer melts have been found to approximately obey the Cox-Merz rule (Venkatraman et al. 1990; Snijkers and Vlassopoulos 2014) relating the equivalence of the steady shear response at a rate $\dot{\gamma}$ and the oscillatory shear response at $\omega = \dot{\gamma}$. We assume that the Cox-Merz rule holds identically and calculates the shear response from the complex viscosity in the linear regime from

$$\eta^*(\omega) = m \omega^{n-1}.$$

The reason we use the linear response is because the pom-pom constitutive model implemented here does not include convective constraint release (CCR) mechanism (Ianniruberto and Marrucci 1996; Milner et al. 2001) for relaxation in the nonlinear flow and shows unstable rate dependence ($n < 0$) for high rates. We report the shear-thinning index and consistency at 1 rad/s (computed from the complex viscosity over frequency range 0.9 rad/s $< \omega < 1.1$ rad/s).

As with the shear viscosity, we define a local power-law that describes the rate dependence of the steady state extensional viscosity by

$$\eta_E(\dot{\epsilon}) = \tilde{m} \dot{\epsilon}^{\tilde{n}-1}$$

For a strictly tension-stiffening material, the “extension-hardening index” \tilde{n} will be larger than 1. We compute $\eta_E(\dot{\epsilon})$

by calculating the transient response in uniaxial extension at extension rate $\dot{\epsilon}$ until a steady state value is reached. The extension-hardening index \tilde{n} is calculated from results in the extension rate interval 0.9/s $< \dot{\epsilon} < 1.1$ /s.

For a shear-thinning melt, often the interest is not in the rate dependence of the absolute magnitude of the extensional viscosity but in some relative importance of the extensional viscosity. For a Newtonian incompressible fluid, the ratio of the extensional viscosity in uniaxial extension and the shear viscosity, the Trouton ratio $T_R = \frac{\eta_E}{\eta} = 3$. The frequency dependence of both the extensional and the shear viscosity necessitates the specification of the rates at which these quantities are measured. For a generalized Newtonian fluid model (inelastic fluid with shear rate dependent viscosity), the ratio of the extensional and shear viscosity remains 3 provided one considers the shear viscosity at a rate that is $\sqrt{3}$ times the rate at which the extensional viscosity is measured (Jones et al. 1987), and the ratio is defined as

$$T_R^E(\dot{\epsilon}) = \frac{\eta_E(\dot{\epsilon})}{\eta(\sqrt{3}\dot{\epsilon})}.$$

For polymer melts, defined in this fashion, the Trouton ratio can be quite large and gives a measure of the relative importance of the elastic nature of the melt. Here, we have added the superscript “E” to highlight that this ratio measures the deviation from inelastic fluid.

Long-chain polymer molecules are stretched in an extensional flow and support additional tension. To isolate this excess stress in extension due to chain stretching, we define another measure of relative extension hardening by comparing the predictions based on the pom-pom constitutive equation

for branched molecules with predictions from a nonstretching constitutive equation. For this, we use the pom-pom model with all the priority variables set to 1. Thus, the comparison is made with a hypothetical melt having identical viscoelastic response in the linear regime but that does not have the additional complexity coming from the molecular structures (chain stretch) relevant in the nonlinear flow of polymer melt. This molecular stretch contribution to the extensional viscosity is expressed as a ratio of steady-state extensional viscosities calculated for both the constitutive models at the same extension rate:

$$\Delta_{ms}(\dot{\varepsilon}) = \frac{\eta_E(\dot{\varepsilon})}{\eta_E^{ns}(\dot{\varepsilon})}.$$

Figure 4 shows the scalar measures for viscoelastic responses as surface and contour plots against the molar masses (M_W^a) and the number of side arms (n^a) of the comb molecules. We use logarithmic scales for both M_W^a and n^a in these figures. The orientation of each plot is independently chosen to highlight the features present. The complex viscosity (Fig. 4a) increases most rapidly with n^a between 0.2 and 2. Melts with a small fractional number of arms mainly consist of star-linear blends. For low-weight fraction of star polymers ($n^a \leq 0.2$), dynamic dilution from the reptation of the linear polymers accelerates the relaxation of the star polymers sufficiently, and the viscosity enhancement is gradual. At $n^a = 2$ (H-polymer), the majority of the molecules are multi-branched. As the number of arms are increased at a fixed molar mass, the final reptative relaxation is slowed down due to the increased friction from the relaxed side arms. However, those side arms provide additional stress relaxation in the hierarchical picture (from their own tube escape, and via dynamic dilution of the stress from the comb backbones), and consequently, beyond $n^a \cong 4$, the complex viscosity starts to gradually decrease with increasing n^a at a fixed M_W^a . The figure shows additional features as a function of M_W^a at a fixed n^a . This is because we have fixed our attention at 1 rad/s. The zero-shear viscosity increases monotonically with M_W^a at fixed n^a .

For small n^a , our comb molecules reach terminal Newtonian regime at 1 rad/s. This shows up as the shear-thinning index $n = 1$ at low n^a in Fig. 4 b. The same is true for small M_W^a . The highest shear-thinning correlates with the parameter space that shows strongest complex viscosity growth. These comb molecules with well-defined architecture show a richer frequency dependence of viscosity than would be obtained for a power-law fluid. The additional features in the plot occur because the different relaxation regimes (arm retraction, Rouse relaxation of backbone with additional friction of relaxed side arms, and reptation) reach our observation window at 1 rad/s as we explore the parameter space.

The extensional viscosity (Fig. 4c) qualitatively mirrors the complex viscosity. The maximum observed as the

number of arms is increased at low arm molar mass due to a competition between increased friction from more side arms and increased dilution of the final relaxation modulus (as with the complex viscosity as described above). Since in the Newtonian regime, flow properties are independent of the rate; the extension-hardening index (\tilde{n}) is one at either low values of M_W^a or low values of n^a (Fig. 4d). For $n^a > 0.2$ and $M_W^a > 4$ kg/mol, the polymers show extension thinning. For $n^a \geq 1$, there is a range of M_W^a where the amount of extension thinning is minimal. For comb polymers, the backbone segments confined between branch points support the stretching in an extensional flow. A minimal value of M_W^a is required for the branches to support this tension. But any additional increase in the M_W^a dilutes the weight fraction of tension-carrying backbone, so there is an optimal range of M_W^a for avoiding extension thinning, indicated by the peak in \tilde{n} as a function of M_W^a at $n^a \geq 1$. Increasing n^a increases the amount of tension that the backbone segments can carry, but at the same time decreases the weight fraction of the backbone segments. For our choice of backbone molar mass and the extension rate, the optimum side arm molar mass is $M_W^a \approx 12$ kg/mol. The increased tension from increasing n^a always wins over dilution of the backbone in our parameter space.

Figure 4 a and c indicate that the variation in extensional viscosity with architecture qualitatively mirrors the corresponding shear viscosity, showing changes of three orders of magnitude across the set of combs considered. However, the effects of the elastic nature of the polymers and of molecular stretching can be sensitively discerned by examining the relative enhancements of the extensional viscosity compared to some theoretical expectation. For example, Fig. 4 e shows the Trouton ratio which would be expected to have a value of 3 for a generalized Newtonian fluid (which is purely viscous). Because the molecules considered here have elastic component, T_R^E is always above 3 and shows a peaked behavior in the same parameter range where the extension-hardening index shows a local maximum. Likewise, Fig. 4 f shows the ratio (Δ_{ms}) of the predicted extensional viscosity to the prediction of an equivalent viscoelastic model that excludes molecular stretching. Δ_{ms} is therefore a measure of the effects of molecular stretch in the comb materials. There is a peaked response in Δ_{ms} , similar to but sharper than in Fig. 4 d and e. This peak arises from the requirement of a minimum M_W^a to support stretching and from the dilution of stretchable backbone at larger values of M_W^a , and indicates the region of parameter space where the considered extension rate is faster than the inverse of the longest stretch relaxation time. In the present case, that stretch relaxation time arises from the backbone

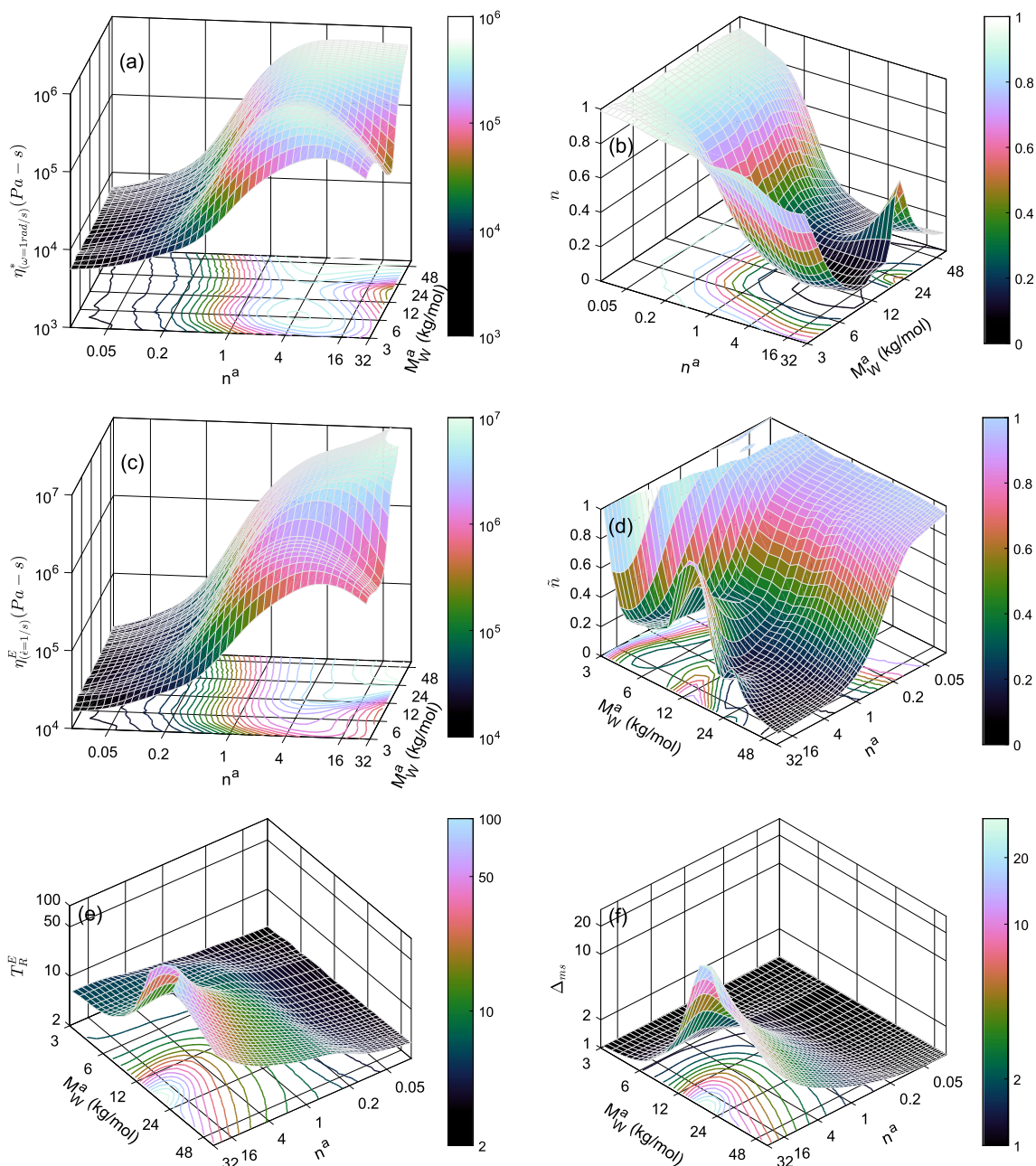


Fig. 4 **a** Complex viscosity, **b** shear-thinning index, **c** extensional viscosity, **d** extension-hardening index, **e** Trouton ratio, and **f** enhancement factor for extensional viscosity from molecular stretch as a function of number of side arms and the molar mass of the side arms

for comb polymers. The shear (extensional) responses are calculated at $\omega = 1 \text{ rad/s}$ ($\varepsilon = 1 \text{ /s}$)

stretch relaxation subject to the friction produced by branch point hopping after side arm relaxation.

Consideration of these different measures permits a useful exploration of parameter space to achieve the desired properties at a relevant flow rate. So, for example, we discover that at flow rates of 1/s, comb with side arm molar mass around 12 kg/mol, and roughly 20 side arms per backbone, gives (i) not too high viscosity, (ii) high shear thinning, but (iii) a strong extensional response (relatively less extension thinning).

Discussions

In this work, we have shown that computational modeling can be used to determine the LCB content in randomly branched polymers by incorporating the knowledge of the synthesis process and all the available measurements, including the flow properties. Inclusion of a model for the polymer synthesis narrows down the possible branching structures and makes it possible to solve the hard inverse problem of finding the

structure of branched polymers from the flow properties. As an example, the linear rheology responses of the metallocene polymers in Fig. 1 could have been explained by considering very specific combinations of linear molecules. However, the frequency dependence of the low frequency elastic modulus shows that the terminal relaxation time of the longest molecules in these polymers must be at least four orders of magnitude longer than the dominant relaxation time from the cross-over frequency of the G' and G'' . The molar mass distribution follows the Flory distribution to good approximation at the large molar mass end (Fig. 1), and the synthesis process does not justify the possibility of having some orders of magnitude longer molecules at low concentrations. Instead, consideration of well-known macromonomer incorporation process (Soares and Hamielec 1996) resulting in small fraction of branched molecules allows us to explain all the available experimental results, including the viscoelastic responses.

We have implicitly assumed that the computational rheology model based on the tube theory provides correct flow responses from the molecular architectures. Though the model has been found to provide satisfactory predictions for the linear and the nonlinear flow properties of a large number of model and industrial polymers, the model is known to have limitations in different scenarios. One severe limitation for the current study is that the model accounts for the temperature as a simple change in the relaxation timescale and the modulus while the experiments on the comb polymers in Fig. 2 show mild thermorheological complexity in the sense that the different temperature responses cannot be made to superpose perfectly with each other. This results in a spread in the response at a particular frequency that in turn increases the uncertainty in our estimates of plateau modulus, or in cross-linking for the comb polymers. The computational model also assumes all inter-branch segments to be well-entangled and expected to perform poorly where this assumption breaks down, for example as for dense combs (Ahmadi et al. 2017).

Since the effect of LCB is much more drastic on the flow properties than that of molar mass, we have mostly used the molar masses of the samples as measured. Our heuristic fitting procedure utilizes qualitative signatures in the flow response (presence of a reptation peak, change in the slope in the frequency response of the elastic modulus, and additional features in the loss modulus) to determine the most likely structures for a particular sample. Complexity in the modeled synthesis is increased incrementally until the model agrees with measurement within the experimental uncertainty. This approach is computationally inexpensive—for a given choice of parameters, prediction of the linear rheology on a personal computer typically takes a few minutes of computation. The qualitative signatures are robust in the sense that they do not penalize the fitting procedure if the absolute value of the predicted rheological response is different from the measured value. This exercise could be formalized as an optimization problem (Takeh et al. 2011), and our

assumption of roughly correct measured molar mass could then be relaxed. In such a scheme, one can also incorporate the unavoidable uncertainty in the experimental measurements and the uncertainty in the model predictions also. But such an approach will require considerably more computational effort (Takeh et al. 2011) and translating the qualitative features, which we can identify as important from experience, to a cost function for the optimization scheme will be difficult.

To predict the nonlinear responses, the model implements a set of uncoupled pom-pom modes with the parameters of the modes determined from the linear rheology calculation. This approximation results in a gradual onset of strain hardening instead of abrupt strain hardening observed experimentally and explained by models (Lentzakis et al. 2014) that accurately capture the coupling of the stretch between the different backbone segments. Also, our implementation of the pom-pom model does not include finite extensibility and will result in qualitatively wrong predictions at extremely fast flows. However, this does not affect the results presented since the rates considered in this study are always much smaller than the inverse of the (bare) Rouse time of the molecules, where strong stretching is anticipated.

Conclusions

In this work, we have shown that computational modeling can integrate knowledge of the synthesis process and different analytical and rheological measurements to give tight bounds on the branching structures of the polymer molecules in a particular sample. We used it to quantify the branching content in metallocene ethylene-1-butene copolymers with extremely low LCB content below 1 in 10^6 carbons. Using the method on a set of comb polymers, we show that solution measurements such as radius of gyration contraction factor can be included in the list of observables to be integrated in the computational scheme.

We have used the computational model to extensively explore the shear and extension responses of model comb polymers. We show that comb polymers do not show strict extension hardening (increasing extensional viscosity with increasing extension rate) in the parameter space explored. However, the long-chain branches in the comb polymers do show much less extension thinning than would be expected from the shear-thinning behavior of the melts. They also demonstrate extension hardening in the sense of a transient extensional viscosity which rises above the linear viscoelastic envelope. We have used multiple scalar variables to visually compare the viscoelastic responses as a function of parameters characterizing the molecules. Such visual representations as a function of parameters characterizing the molecules or parameters controlling the polymer synthesis can be used for other polymers as a guide in finding the optimum structures or synthesis conditions for some particular application.

Acknowledgments The computation for this work was undertaken on ARC2, part of the high-performance computing facilities at the University of Leeds, UK.

Appendix

Experimental details for characterization of the metallocene polymers

Size-exclusion chromatography (SEC) measurements: Molar masses of the polymers were determined from SEC measurements using Agilent 220 °C high temperature unit with three Polymer Laboratories Mixed B columns operating at 145 °C and with 1,2,4 trichlorobenzene as the mobile phase. The SEC setup includes online differential refractometer (DRI), a viscometer, and a multi-angle laser light scattering (MALLS) detector. The details of the detector design and calibration were presented by Sun et al. (2004). As expected for predominantly linear polymers, except at the ends of the elution volumes, the molar mass values determined from the DRI calibration curve and the LS detector agree with each other. To avoid uncertainty associated with the calibration curve, we used the results from the LS detector in determining the molar mass distribution presented in Fig. 1. Polynomial extrapolations to the logarithms of the molar mass and the elution volume were used to assign molar mass values outside the sensitive range of the LS detector.

Small amplitude oscillatory shear (SAOS) experiments: Approximately 1-mm-thick discs of the samples were prepared by compression molding under vacuum. The linear viscoelastic responses were measured at 190 °C under nitrogen atmosphere using an Advanced Rheometric Expansion System (ARES G2, TA Instruments) rheometer with 25-mm parallel plates. Care was taken to ensure that the measurements were limited to the linear regime and the samples do not degrade during the measurement. Error estimates in the measured viscous and elastic moduli were calculated using the transducer sensitivity and were found to be smaller than the symbol sizes used in Fig. 1. Repeat measurements were performed for PEL113 at 150 °C. The results from the two temperature measurements can be superposed using a frequency shift. In particular, the slope of the elastic modulus was found to be robust and cannot be attributed to experimental artifact.

Open Access This article is distributed under the terms of the Creative Commons Attribution 4.0 International License (<http://creativecommons.org/licenses/by/4.0/>), which permits unrestricted use, distribution, and reproduction in any medium, provided you give appropriate credit to the original author(s) and the source, provide a link to the Creative Commons license, and indicate if changes were made.

Publisher's note Springer Nature remains neutral with regard to jurisdictional claims in published maps and institutional affiliations.

References

- Ahmadi M, Pioge S, Fustin C-A, Gohy J-F, van Ruymbeke E (2017) Closer insight into the structure of moderate to densely branched comb polymers by combining modelling and linear rheological measurements. *Soft Matter* 13:1063–1073
- Ball RC, McLeish TCB (1989) Dynamic dilution and the viscosity of star polymer melts. *Macromolecules* 22:1911–1913
- Braunschweig H, Breitling FM (2006) Constrained geometry complexes—synthesis and applications. *Coord Chem Rev* 250:2691–2720
- Britovsek GJP, Gibson VC, Wass DF (1999) The search for new-generation olefin polymerization catalysts: life beyond metallocenes. *Angew Chem Int Ed* 38:428–447
- Carrot C, Guillet J (1997) From dynamic moduli to molecular weight distribution: a study of various polydisperse linear polymers. *J Rheol* 41:1203–1220
- Chambon P, Fernyhough CM, Im K, Chang T, Das C, Embery J, McLeish TCB, Read DJ (2008) Synthesis, temperature gradient interaction chromatography, and rheology of entangled styrene comb polymers. *Macromolecules* 41:5869–5875
- Chang T (2005) Polymer characterization by interaction chromatography. *J Polym Sci B Polym Phys* 43:1591–1607
- Chen X, Stadler FJ, Münstedt H, Larson RG (2010) Method for obtaining tube model parameters for commercial ethene/ α -olefin copolymers. *J Rheol* 54:393–406
- D'Agnillo L, Soares JBP, Penlidis A (2002) Round-robin experiment in high-temperature gel permeation chromatography. *J Polym Sci B Polym Phys* 40:905–921
- Daniels DR, McLeish TCB, Crosby BJ, Young RN, Fernyhough CM (2001) Molecular rheology of comb polymer melts. 1. Linear viscoelastic response. *Macromolecules* 34:7025–7033
- Das C, Read DJ (2018) bob2.5. <http://sourceforge.net/projects/bob-rheology>. Accessed 11 June 2018
- Das C, Inkson NJ, Read DJ, Kelmanson MA, McLeish TCB (2006) Computational linear rheology of general branch-on-branch polymers. *J Rheol* 50:207–234
- Das C, Read DJ, Auhl D, Kapnistos M, den Doelder J, Vittorias I, McLeish TCB (2014) Numerical prediction of nonlinear rheology of branched polymer melts. *J Rheol* 58:737–757
- de Gennes PG (1971) Reptation of a polymer chain in the presence of fixed obstacles. *J Chem Phys* 55:572–579
- Dealy JM, Read DJ, Larson RG (2018) Structure and rheology of molten polymers. Hanser, Munich
- des Cloizeaux J (1988) Double reptation vs simple reptation in polymer melts. *Europhys Lett* 5:437–442
- Doi M, Edwards SF (1986) The theory of polymer dynamics. Clarendon Press, Oxford
- Fernyhough CM, Young RN, Poche D, Degroot AW, Bosscher F (2001) Synthesis and characterization of polybutadiene and poly(ethylene-1-butene) combs. *Macromolecules* 34:7034–7041
- Fetters LJ, Lohse DJ, García-Franco CA, Brant P, Richter D (2002) Prediction of melt state poly(α -olefin) rheological properties: the unsuspected role of the average molecular weight per backbone bond. *Macromolecules* 35:10096–10101
- Frischknecht AL, Milner ST, Pryke A, Young RN, Hawkins R, McLeish TCB (2002) Rheology of three-arm asymmetric star polymer melts. *Macromolecules* 35:4801–4820
- Gortis AD, Zeevenhoven BLF, Hogt AH (2004) The effect of long chain branching on the processability of polypropylene in thermoforming. *Polym Eng Sci* 44:973–982
- Hadjichristidis N, Xenidou M, Iatrou H, Pitsikalis M, Poulos Y, Avgeropoulos A, Sioula S, Paraskeva S, Velis G, Lohse DJ, Schulz DN, Fetters LJ, Wright PJ, Mendelson RA, Gracia-Franco CA, Sun T, Ruff CJ (2000) Well-defined, model long chain

- branched polyethylene. 1. Synthesis and characterization. *Macromolecules* 33:2424–2436
- Hatzikiriakos SG (2000) Long chain branching and polydispersity effects on the rheological properties of polyethylenes. *Polym Eng Sci* 40:2279–2287
- Hutchings LR, Kimani SM, Hoyle DM, Read DJ, Das C, McLeish TCB, Chang T, Lee H, Auhl D (2012) In silico molecular design, synthesis characterization, and rheology of dendritically branched polymers: closing the design loop. *ACS Macro Lett* 1:404–408
- Ianniruberto G, Marrucci G (1996) On compatibility of the Cox-Merz rule with the model of Doi and Edwards. *J Non-Newtonian Fluid Mech* 65:241–246
- Inkson NJ, Graham RS, McLeish TCB, Groves DJ, Fernyhough CM (2006) Viscoelasticity of monodisperse comb polymer melts. *Macromolecules* 39:4217–4227
- Janzen J, Colby RH (1999) Diagnosing long-chain branching in polyethylenes. *J Mol Struct* 485–486:569–584
- Jones DM, Walters K, Williams PR (1987) On the extensional viscosity of mobile polymer solutions. *Rheol Acta* 26:20–30
- Kapnistos M, Vlassopoulos D, Roovers J, Leal LG (2005) Linear rheology of architecturally complex macromolecules: comb polymers with linear backbones. *Macromolecules* 38:7852–7862
- Larson RG (2001) Combinatorial rheology of branched polymer melts. *Macromolecules* 34:4556–4571
- Le'onardi F, Allal A, Martin G (2002) Molecular weight distribution from viscoelastic data: the importance of tube renewal and Rouse modes. *J Rheol* 46:209–224
- Lentzakis H, Das C, Vlassopoulos D, Read DJ (2014) Pom-pom-like constitutive equations for comb polymers. *J Rheol* 58:1855–1875
- Li SW, Lee H, Park H, Dealy J, Milan M, Im K, Choi H, Chang T, Rahman M, Mays J (2011) Detecting structural polydispersity in branched polybutadienes. *Macromolecules* 44:208–214
- Liu Y, Shaw MT, Tuminello WH (1998) Obtaining molecular-weight distribution information from the viscosity data of linear polymer melts. *J Rheol* 42:453–476
- Lohse DJ, Milner ST, Fetters LJ, Xenidou M, Hadjichristidis N, Mandelson RA, Gracia-Franco CA, Lyon MK (2002) Well-defined, model long chain branched polyethylene. 2 Melt rheological behaviour. *Macromolecules* 35:3066–3075
- Marrucci G (1985) Relaxation by reptation and tube enlargement: a model for polydisperse melts. *J Polym Sci Polym Phys Ed* 23:159–177
- McLeish TCB (1988) Hierarchical relaxation in tube models of branched polymers. *Europhys Lett* 6:511–516
- McLeish TCB, Larson RG (1998) Molecular constitutive equations for a class of branched polymers: the pom-pom polymer. *J Rheol* 42:81–110
- Milner ST, McLeish TCB, Likhthman AE (2001) Microscopic theory of convective constraint release. *J Rheol* 45:539–563
- Münstedt H, Steffl T, Malmberg A (2005) Correlation between rheological behaviour in uniaxial elongation and film blowing properties of various polyethylenes. *Rheol Acta* 45:14–22
- Pattamaprom C, Larson RG, Sirivat A (2008) Determining polymer molecular weight distributions from rheological properties using the dual-constraint model. *Rheol Acta* 47:689–700
- Randall JC (2006) A review of high resolution liquid ¹³C nuclear magnetic resonance characterizations of ethylene-based polymers. *J Macromol Sci C Polym Rev* 29:201–317
- Read DJ, McLeish TCB (2001) Molecular rheology and statistics of long chain branched metallocene-catalyzed polyolefins. *Macromolecules* 34:1928–1945
- Read DJ, Auhl D, Das C, den Doelder J, Kapnistos M, Vittorias I, McLeish TCB (2011) Linking models of polymerization and dynamics to predict branched polymer structure and flow. *Science* 333:1871–1874
- Sebastian DH, Dearborn JR (1983) Elongation rheology of polyolefins and its relation to processability. *Polym Eng Sci* 23:572–575
- Shroff RN, Mavridis H (1999) Long-chain-branching index for essentially linear polyethylenes. *Macromolecules* 32:8454–8464
- Slootmaekers D, van Dijk JAPP, Varkevisser FA, van Treslong CJB, Reynaers H (1991) Molecular characterisation of κ - and λ -carrageenan by gel permeation chromatography, light scattering, sedimentation analysis and osmometry. *Biophys Chem* 41:51–59
- Snijkers F, Vlassopoulos D (2014) Appraisal of the Cox-Merz rule for well-characterized entangled linear and branched polymers. *Rheol Acta* 53:935–946
- Snijkers F, van Ruymbeke E, Kim P, Lee H, Nikopoulou A, Chang T, Hadjichristidis N, Pathak J, Vlassopoulos D (2011) Architectural dispersity in model branched polymers: analysis and rheological consequences. *Macromolecules* 44:8631–8643
- Soares JBP, Hamielec AE (1996) Bivariate chain length and long chain branching distribution for copolymerization of olefins and polyolefin chains containing terminal double-bonds. *Macromol Theory Simul* 5:547–572
- Stadler FJ, Münstedt H (2008) Terminal viscous and elastic properties of linear ethene/alpha-olefin copolymers. *J Rheol* 52:697–712
- Sun T, Chance RR, Graessley WW, Lohse DJ (2004) A study on the separation principle in size exclusion chromatography. *Macromolecules* 37:4304–4312
- Takeh A, Worch J, Shanbhag S (2011) Analytical rheology of metallocene-catalyzed polyethylenes. *Macromolecules* 44:3656–3665
- van Ruymbeke E, Stéphenne V, Daoust D, Godard P, Keunings R, Bailly C (2005) A sensitive method to detect very low levels of long chain branching from the molar mass distribution and linear viscoelastic response. *J Rheol* 49:1503–1520
- van Ruymbeke E, Bailly C, Keunings R, Vlassopoulos D (2006) A general methodology to predict the linear rheology of branched polymers. *Macromolecules* 39:6248–6259
- van Ruymbeke E, Kaivez A, Hagenars A, Daoust D, Godard P, Keunings R, Bailly C (2006a) Characterization of sparsely long chain branched polycarbonate by a combination of solution, rheology and simulation methods. *J Rheol* 50:949–973
- van Ruymbeke E, Lee H, Chang T, Nikopoulou A, Hadjichristidis N, Snijkers F, Vlassopoulos D (2014) Molecular rheology of branched polymers: decoding and exploring the role of architectural dispersity through a synergy of anionic synthesis, interaction chromatography, rheometry and modelling. *Soft Matter* 10:4762–4777
- Venkatraman S, Okano M, Nixon A (1990) A comparison of torsional and capillary rheometry for polymer melts: the Cox-Merz rule revisited. *Polym Eng Sci* 30:308–313
- Wang W-J, Kharchenko S, Migler K, Zhu S (2004) Triple-detector GPC characterization and processing behavior of long-chain-branched polyethylene prepared by solution polymerization with constrained geometry catalyst. *Polymer* 45:6495–6505
- Wood-Adams P, Costeux S (2001) Thermorheological behavior of polyethylene: effects of microstructure and long chain branching. *Macromolecules* 34:6281–6290
- Zimm BH, Stockmayer WH (1949) The dimensions of chain molecules containing branches and rings. *J Chem Phys* 17:1301–1314